Guiding and scattering of ions in transmission through mica nanocapillaries

H. Q. Zhang (张红强),[1,2,*] N. Akram,[1] and R. Schuch[1,†]
[1]*Physics Department, Stockholm University, S-106 91 Stockholm, Sweden*
[2]*School of Nuclear Science and Technology, Lanzhou University, Lanzhou 730000, China*
(Received 3 May 2016; published 7 September 2016)

The transition from guiding to scattering in the transmission of 70-keV Ne^{7+} through mica nanocapillaries of rhombic cross section is studied. Transmitted ions and neutrals are separated and their angular distributions are measured for various tilt angles of the capillaries with respect to the beam direction. The ions and neutrals have different angular profiles and different transmission dependences on tilt angle. The profiles of the transmitted ions are of rectangular shape while bananalike shapes appear for the neutrals. The time evolution measurements during charging up show a shift of the center of the ion angular distribution while that of the neutrals remains fixed. Trajectory simulations are performed by taking the image force and the Coulomb repulsive force from the deposited charge, as well as scattering from capillary walls into account. These show good agreement with the data and how the deposited or image charge deflects and shapes the ionic portion of the beam differently from the neutral part. The experimental separation of the ions from neutrals and their very different behaviors together with simulations gives us further insight into the mechanisms of guiding and scattering in transmission through nanocapillaries.

DOI: 10.1103/PhysRevA.94.032704

I. INTRODUCTION

The transmission of slow, highly charged ions (HCIs) through insulating nanocapillaries has been studied in various configurations since the so-called guiding effect was found [1–31]. The characteristic features are that the bulk of transmitted ions leave the capillaries in their orientation, remaining in their initial charge state and kinetic energy. This guiding phenomenon was first found in nanocapillaries in polyethylene terephthalate (PET) [1] and later observed in many other insulating materials such as SiO_2,Al_2O_3, and polycarbonate (PC) by different groups [4–9]. Also, single, macroscopic capillaries of borosilicate glass were used to make microbeams [15–18]. Transmission of electrons through nanocapillaries in PET and Al_2O_3 [19,20,24] was also studied.

The guiding mechanism is attributed to charge deposition by ion impact on the capillary walls. These deposited charge patches avoid close wall collisions of subsequent ions and transmit them along the axis of the capillaries. The formation of the charge patches happens in a self-arranged, time-dependent manner resulting in increased transmission of ions until an equilibrium is reached. The equilibrium refers to a steady state between deposition of charges on the capillary walls and drainage of charges through numerous discharging channels. A small number of charge patches are guiding the ions through the nanocapillaries [25]. This was revealed in systematic studies of the temporal evolution of the transmitted ions showing an oscillatory angular distribution [26–28]. In addition, it was confirmed by Monte Carlo simulations that reproduced the sequential formation of charge patches inside the capillaries and gave essential insight into the guiding phenomenon [21–23].

All previous studies on the guiding of HCIs through insulating nanocapillaries have utilized capillaries of circular cross sections. There the shape of the angular distribution of transmitted ions is only determined by the aspect ratio and the tilt angle of the capillaries with respect to the beam. We have been able to fabricate micromembranes of mica having uniform nanocapillaries of various cross sections. By using nanocapillaries of rhombic and rectangular cross sections, we revealed influences from the geometrical shape of the guiding channels on the ion transmission profile [28]. For small tilt angles (smaller than the aspect ratio of the capillaries), it was found that capillaries of rhombic cross section produce rectangular-shaped ion transmission profiles and, vice versa, capillaries of rectangular geometry give a rhombic beam shape [28].

Starting from completely discharged capillaries, the immediate onset of the transmitted intensity with unchanging angular distribution indicates an instant interaction, not governed by deposited charges. Our trajectory simulations confirm that the observed shaping effect is due to the image forces induced by the ions passing through the nanocapillaries. The projectiles gain transverse energy due to the image charge attraction and therefore their kinetic energy increases a bit from the incident energy [31]. This leads to a defocusing of the ions leaving the capillaries. Due to the blocking of large deflection angles at the exit of the capillary, the transmitted ion beam is tailored into certain geometrical patterns.

In Monte Carlo simulations of ion guiding through insulating nanocapillaries of circular cross section, no clear effect of the image charge has been identified [21,22]. Beam shaping by image charge forces is an instantaneous process, contrary to the time-dependent ion-guiding effect due to gradual charging up of the capillary walls before reaching equilibrium between deposition and drainage of charges. The defocusing of the beam by the image force should act also in circular capillaries and could be the cause for the broadening of the angular distributions, seen in several guiding experiments [2–4,7,9,12,13].

In this work, we report about quite different features of the transport of 70-keV Ne^{7+} ions through rhombic capillaries in a muscovite mica membrane [29,30] that exit the capillaries either fully charged or completely neutralized. The fraction

*zhanghq@lzu.edu.cn
†schuch@fysik.su.se

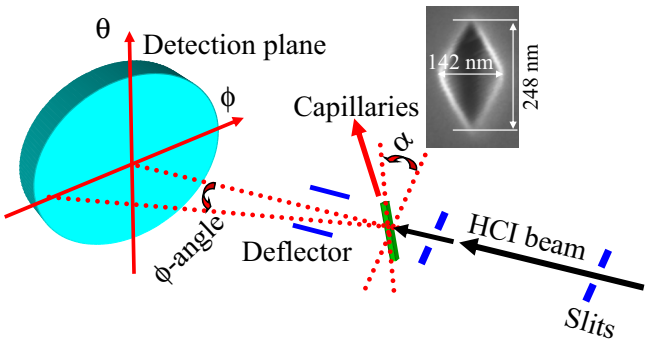

FIG. 1. A schematic view of the setup for the ion transmission experiments (inset shows SEM scan of one of the rhombic nanocapillaries).

of transmitted charged or neutral particles is shown to change with the tilt angle of the capillaries and with the time (incident charge) evolution. We find also dramatically different angular distributions of neutral and charged particles transmitted through rhombic nanocapillaries. Trajectory simulations are performed to explain the results. And, based on these simulations, the observations with charge separated particles after transmission through the capillaries gives us further insight into the guiding phenomena.

II. EXPERIMENTS

The transmission experiments with HCIs were performed at the ECR ion source and S-EBIT of Stockholm University (schematic view, Fig. 1). Beams of 70-keV Ne^{7+} ions were collimated by pairs of slits to a size of 2×2 mm^2, leading to a divergence of less than 0.1°. The current was in the range of 30–250 pA/mm^2 impinging on the capillary membrane. The transmitted projectiles were detected using microchannel plates (MCPs) with a two-dimensional resistive anode. The detector signals and beam intensity were recorded in event mode by a multiparameter data acquisition system [25,28]. A pair of parallel plates was put between the capillary membrane and the detector to separate the charge state of the transmitted particles.

The capillary membrane was mounted on a goniometer allowing independent adjustment in three spatial directions and around two rotational axes. The capillaries are aligned with respect to the beam direction and their orientation is described by the tilt angle α. The detection angles, ϕ and θ, are specified with respect to the incident beam direction (see Fig. 1). The angles are experimentally defined in the same way as in our previous work [25,28].

The scanning electron microscope (SEM) scan of one of the rhombic nanocapillaries shows the geometry of them (inset, Fig. 1). The rhombic capillaries have acute angles of 60° and obtuse angles of 120° with a long axis of 248 nm and a short axis of 142 nm, and a channel length of 20 μm which gives the geometrical opening angle of 0.4° for the short axis and 0.7° for the long axis. The low geometrical transparency (porosity) of capillaries (0.9%) in the mica membrane ensures that the capillaries can be regarded as the individual well-separated objects. To avoid macroscopic charge up, Au films of 10 nm thickness were evaporated on both sides. More details of the mica capillaries can be found in our previous work [29,30].

III. RESULTS

A. Transmitted angular distributions at various tilt angles

The angular distributions in the stationary state of transmission for 70-keV Ne^{7+} impinging on mica nanocapillaries of rhombic cross section are shown in Fig. 2 for various tilt angles. The top row shows the angular distributions without deflection; bottom row: a deflection voltage of 400 V is applied to a pair of parallel plates after the capillary membrane. Each image from the measurements is taken for the incident charge of 280 e per capillary (the incident charge per capillary) for the tilt angle of +0.4°, + 0.9°, and –0.6° after the stationary state of the transmission is reached. For the other tilt angles in the graph, the images correspond to an accumulation of the incident charge of 1400 e per capillary. The center of the

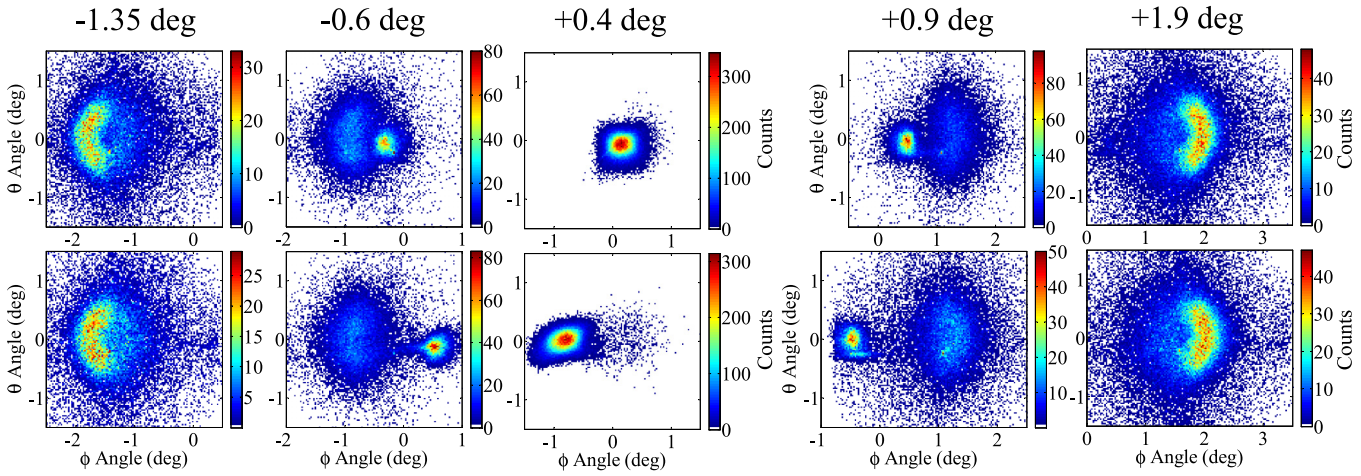

FIG. 2. Two-dimensional transmitted angular distributions for 70-keV Ne^{7+} ions through rhombic capillaries for various tilt angles at the stationary state of transmission. Top: angular distributions without deflection; bottom: deflected by a voltage of 400 V. For the tilt angle of +0.4°, + 0.9°, and –0.6°, the images correspond to an accumulation of the incident charge of 280 e per capillary; for the other tilt angles in the graph, the images are for an accumulated incident charge of 1400 e per capillary.

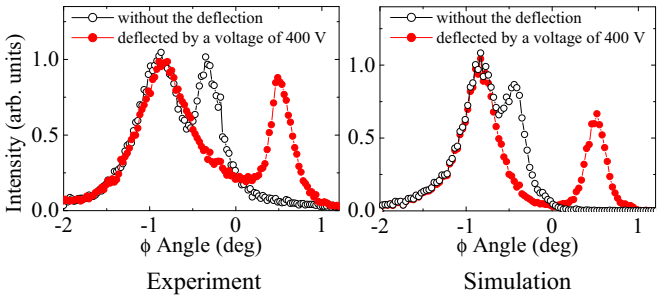

FIG. 3. Projections of the transmitted angular distributions onto the ϕ plane at the tilt angle of –0.6°. (Left) the experimental projection at the stationary state of transmission; (right) the simulated projection for the deposited charge of 4200 e per capillary (see Sec. IV). Deflection voltage was 400 V.

angular distribution of the transmitted ions is separated from that of the neutrals by 0.95°, (bottom row) by the deflection voltage of 400 V. As seen in Fig. 2, the transmitted ions are tailored into a rectangular shape, with the long sides aligned along the short axes of the rhombi (as reported previously [29]), at small tilt angles (less than the geometrical opening angle). At tilt angles larger than the geometrical opening angle the neutrals are found in a bananalike shape (see Fig. 2).

For the neutrals, the center of the angular distributions follows the change of the tilt angle as seen in Fig. 2, where they are seen centered at angles larger than the tilt angle, lying in the range from the tilt angle to the angle away from it by the geometrical opening angle. For ions, the angular distribution is centered around the angles smaller than the tilt angle, i.e., as shown clearly by projections of the transmitted angular distributions onto the ϕ plane at the tilt angle of –0.6° in Fig. 3.

The transmission rates (the amount of the transmitted projectiles normalized to a certain amount of the incoming ions) as a function of the tilt angle for the neutrals and ions are shown in Fig. 4. As seen in the figure, a double peak structure occurs for the transmission rate of the neutrals as a function of the tilt angle. The peaks are around the tilt angle at which the capillary just geometrically blocks the beam, i.e., above the geometrical opening angle (0.4°) plus the beam divergence

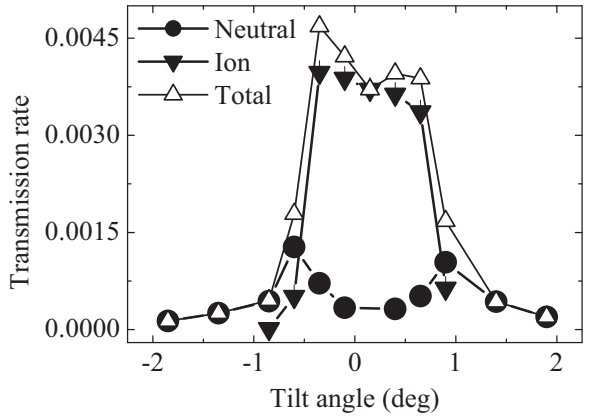

FIG. 4. Transmission rates of ions and neutrals at various tilt angles for 70-keV Ne^{7+} ions hitting mica nanocapillaries of rhombic cross section.

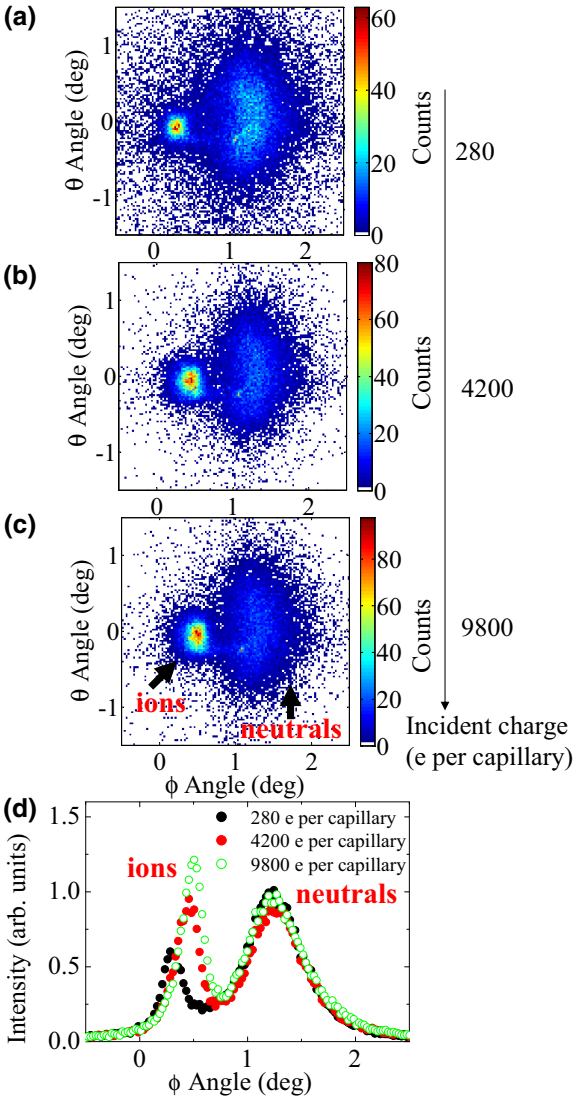

FIG. 5. Two-dimensional angular distribution of 70-keV Ne^{7+} transmitted through mica nanocapillaries of rhombic cross section during charging up [integrated charge: (a) 280 e per capillary; (b) 4200 e per capillary; (c) 9800 e per capillary; denoted on the right side], at tilt angle +0.9° after rotating from +1.4°. In (d) are the corresponding projections of the transmitted angular distributions (a–c) onto the ϕ plane.

(0.1°). The transmission rate of the ions is roughly constant at tilt angles within the aspect ratio and drops fast to zero outside, where the capillary is not geometrically transparent to the beam. At larger tilt angles, there are no ions but only neutrals in the transmitted angular distributions. This comes from the fact that different mechanisms are responsible for transport of ions and neutrals through the capillaries.

B. Time (incident charge) evolution of the angular distributions

1. Charged capillaries

The time (incident charge) evolution of the angular distribution of transmitted particles, measured at the tilt angle of +0.9° during charging up after rotating from +1.4°, is shown in Fig. 5. The center of the angular distribution for

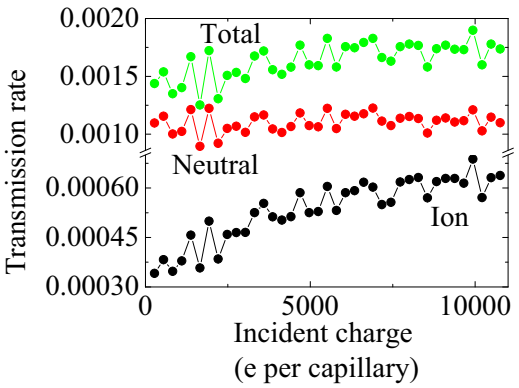

FIG. 6. The experimental transmission rate is plotted for the ions and neutrals, as denoted in the figure, as a function of the incident charge (e per capillary) at the tilt angle of $+0.9^\circ$, after rotating from $+1.4^\circ$.

neutrals ($+1.2^\circ$) lies at larger angles than the tilt angle while for ions it peaks at angles smaller than the tilt angle [see Fig. 5(d)]. The ionic portion shifts towards the tilt angle while the center of the angular distribution for the neutrals remains the same during charging up (see Fig. 5). The transmission rate for ions increases with time (incident charge) but for neutrals, the transmission rate remains constant, as shown in Fig. 6.

2. *Discharged capillaries*

In order to study the influence of the deposited charges on the transmitted neutrals and ions, the time (incident charge) evolution of the angular distributions of transmitted particles was measured at the tilt angle of –0.6° during charging up of the initially discharged capillaries. We separated the ions from the neutrals by 400 V applied to the parallel plates (as mentioned above, this deflects 70-keV Ne^{7+} by 0.95°). The

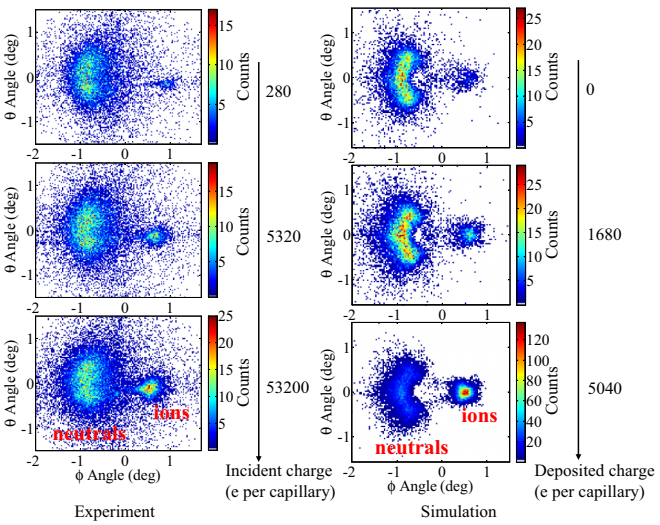

FIG. 7. Time evolution of the angular distributions for 70-keV Ne^{7+} transmitted through rhombic capillaries at various stages during charging up at the tilt angle of –0.6° (experimental left, simulations right). A voltage of 400 V is applied to the deflector to separate transmitted ions from neutrals.

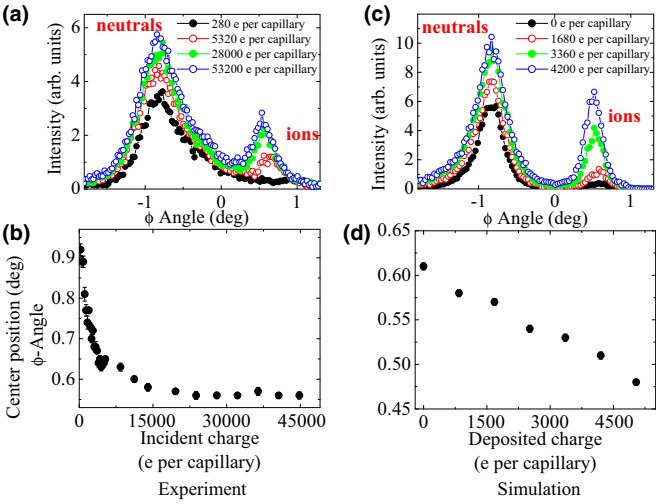

FIG. 8. Projections of the transmitted angular distributions onto the ϕ plane: (a) experimental for various incident charges during charging up; (c) simulations for various deposited charges. Center positions of the angular distributions of the transmitted ions (from the ϕ projection) are plotted in (b,d) as a function of the incident charge (experiment) and the deposited charge (simulation), respectively. The plots are for a tilt angle of –0.6° and for initially uncharged capillaries. The deflector was set at a voltage of 400 V to separate the transmitted ions from the neutrals.

results are shown in Figs. 7–9. In Fig. 7, it can be seen that in the beginning of charging up, the ions appear at angles smaller than the tilt angle plus the deflection angle ($+0.95^\circ$), then the ions shift towards the tilt angle.

As seen in the projections of the transmission profiles onto the ϕ plane (Fig. 8), the ionic portion shifts from $+0.9^\circ$ to $+0.55^\circ$ (note that these angles include $+0.95^\circ$ by the deflector), towards the tilt angle [Figs. 8(a) and 8(b)]. The center of the angular distribution for the neutrals remains at the same value of -0.84° during charging up. The transmission rate of the ions increases with time (incident charge), as well as that of the neutrals [see Fig. 9(a)]. The transmission rate as a function of time (incident charge) is different from that for charged capillaries as shown in Fig. 6, suggesting that the deposited charge from previous tilt angles complicates the observations. Therefore, a better defined study should exclude

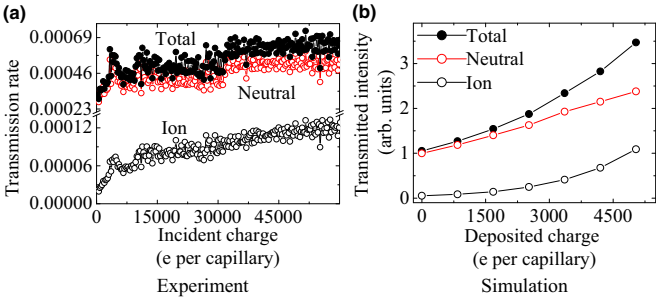

FIG. 9. Experimental transmission rates (left) and simulated transmission intensities (right) of ions and neutrals at the tilt angle of –0.6° are plotted as a function of the incident charge (a) and the deposited charge (b), respectively, for initially uncharged capillaries.

this by using discharged capillaries. However, we observe that the ionic portion shifts towards the tilt angle whereas the center of the angular distribution for the neutrals remains the same during charging up for both charged capillaries and discharged capillaries. This is different from previous work [14], where 3-keV Ar^{7+} ions are guided through polyethylene terephthalate nanocapillaries.

IV. SIMULATIONS AND DISCUSSIONS

In order to quantitatively describe the observed phenomena, we performed trajectory simulations by taking into account three processes: (1) deflection by the image force; (2) deflection due to Coulomb repulsive force from the deposited charges; (3) scattering of the particles from the capillary surfaces.

A. Method of the simulation

The calculation of the electric field from the deposited charge is the same as presented in our previous work [30]. The capillary walls are divided into rectangular strips. The electric field experienced by the ion is a sum of the fields from the deposited charge on these strips. A static surface charge distribution is used while the total amount of the deposited charge varies with the number of ions hitting the walls. The static charge distribution originates from the geometrical hit probability distribution on the capillary walls by a Gaussian beam with the same divergence as the experimental value.

The simplest form of the image force is used in the simulation. The net force on the projectile is taken into account in the first order by superposition of the image forces from each side of the nanocapillary wall [29–31].

A simple statistical model is formulated to simulate the scattering of the projectiles from the surface of the capillaries to avoid calculating detailed trajectories for the collisions with the surface. There are four mechanisms involved: deflection from the surface, scattering of the projectiles, charge exchange processes, and surface roughness.

The probability of scattering from the surface is determined by assuming the ion moves in an average planar potential as follows [32]:

$$P_r(\varphi) = \exp(-E\sin^2\varphi/U_0), \tag{1}$$

where E is the projectile kinetic energy; φ is the angle of the projectile with respect to the inner surface of the capillary at the impact site; U_0 is the surface potential from an average planar potential as follows:

$$U_0 = 2\pi Z_p Z_t n_a a_s \sum_{i=1}^{3} \frac{c_i}{d_i}, \tag{2}$$

where Z_p and Z_t are the projectile and target nuclear charges, respectively; n_a is the surface density of target atoms per unit area; and $c_i = \{0.35, 0.55, 0.1\}$ and $d_i = \{0.3, 1.2, 6\}$ are Molière parameters [32]. The screening length a_s is given by

$$a_s = 0.888(\sqrt{Z_p} + \sqrt{Z_t})^{-2/3}. \tag{3}$$

The scattering angles of the projectiles are assumed to be determined by Firsov scattering. Firsov formulated the scattering angle distribution for grazing incidence ions as follows [33]:

$$P(\varphi,\beta) = \frac{3}{2\pi}\frac{(\varphi\beta)^{3/2}}{\varphi(\varphi^3+\beta^3)}, \tag{4}$$

where φ is the projectile incident angle with respect to the surface and β the scattering angle. Figure 10 shows the scattering angle distribution at the incident angle of 2° from Eq. (4). As it can be seen, the scattering angle of the projectiles is centered at 2°. This is similar to specular reflection.

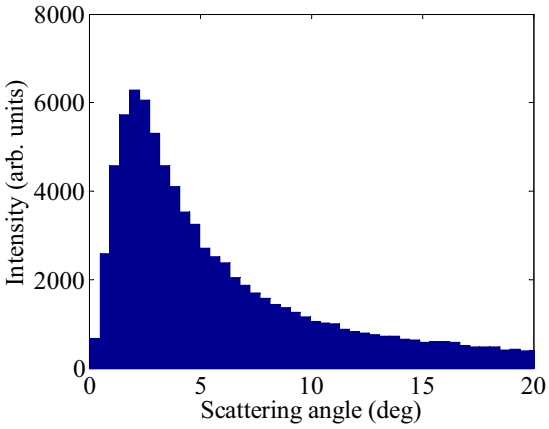

FIG. 10. The scattering angle distribution at the incident angle $\varphi = 2^\circ$ from a surface given by the Firsov formula (see the text).

To include charge exchange processes in case of deflection, the classical over barrier model is applied (see [34] and the reference therein). In the case where the projectile is scattered from the surface, we assume it is being neutralized. The surface roughness is also taken into account by random sampling the angle of the surface normal of the inner wall of the capillary at the local collision site.

In the trajectory calculations, the projectile parameters are generated and tracked from the entrance of the capillary. The projectile experiences the image force and the Coulomb force from the deposited charge when it is above the surface in the channel. When the projectile hits the wall of the capillary, the reflection from the surface is decided by comparing a random generated number with the reflection probability P_r [Eq. (1)]. For the scattered and fully neutralized projectile, the reflection angle is obtained from the Firsov formula [Eq. (4)].

B. Simulated results and discussion

For clarity, the simulations are performed for charging up initially uncharged capillaries and registering transmitted ions and neutrals at the tilt angle of –0.6°. The results are shown in Figs. 3 and 7–9. As can be seen in Fig. 7, the simulated transmitted angular distributions agree well with the experimental ones. The banana-shaped profile for the neutrals is reproduced. The projections of the transmission profiles onto the ϕ plane (Fig. 8) and the centers of the transmitted neutrals and ions from the simulation are very close to those of the experiment. The neutrals, mostly from single scattering from the inner surfaces of the capillaries, are centered at the angle of –0.83°, quite close to the experimental value of –0.84° (Fig. 8). The shift of the angular distributions for the ions found in the

simulation compares well to the experiment [see Figs. 8(b) and 8(d)], but the range of the shift is smaller in the simulation than in the experiment. One can see that there is a large quantitative difference between the amounts of deposited charge in the simulation compared to the incident charge in the experiment. We think the reason for that is (i) not all incident charge leads to deposited charge on the surface of the capillaries; (ii) deposited charge is *smaller* due to various discharge channels.

The simulated transmission rate as a function of the deposited charge reaches a faster saturation for the neutrals than for the ions. An indication for this is also seen in the experiment (Fig. 9). As mentioned above, it is found in the simulation that the neutrals are from single scattering at the inner surface of the capillary. Therefore, the most probable scenario is that the increase of the strength of the deflection field from the deposited charge leads to an increase of the number of incident ions that hit the inner surface at smaller φ angles; this leads thus to an increase of the transmission rate of neutrals during charging up [as indicated in Eq. (1)]. This process accelerates faster than the deflection of the ions to the exit of the channels that leads to the increase of the transmission rate for ions. For a semiquantitative comparison, the projections of the simulated angular distributions at 4200 *e*/capillary deposited charge are plotted in Fig. 3(b) together with the experimental projections in the stationary state of the transmission [Fig. 3(a)]. Good agreement is found between simulation and experiment, considering the simplicity of the simulation.

V. SUMMARY AND CONCLUSIONS

By detecting angular distributions of neutrals and ions we identified different mechanisms of ion transport through nanocapillaries in insulator membranes. This has been in particular possible by using mica nanocapillaries of rhombic cross section and changing their tilt angle with respect to the beam direction over a wide range. The angular profile of transmitted particles shows two distinct patterns: One is the rectangular shape from the ions; the other is the bananalike shape from the neutrals. The bananalike shape observed for the neutrals resembles the behavior seen previously in small-angle ion-surface scattering [34,35]. A double peak structure is found for the transmission rate of the neutrals as a function of tilt angles. The time evolution measurement shows that the ionic beam shifts while the center of the angular distribution of the neutrals remains fixed during charging up. In contrast, the transmission rate increases both for ions and neutrals as a function of the accumulated incident charge (time).

Trajectory simulations are performed by taking account of the image force and the Coulomb repulsive force from the deposited charge, as well as scattering, to understand the transmission patterns seen in the experiment. Thereby we find that the bananalike shape of the neutrals is from single scattering at the inner surface of the capillary, and the rectangular shape of the ions comes from tailoring by the image force, as well as the shift of the ionic angular distributions from deflection of the ions by the deposited charge. The scattering and neutralization occurs with an essential fraction for incident ions with angles larger than the aspect ratio and energy of several tens of keV. The transmission characteristics can be very different for lower or higher incident energies. Therefore, when it comes to scaling laws for transmission rates, guiding strength, and angular widths for ion guiding in capillaries, attention should be paid to separate ions from neutrals for their characterization.

ACKNOWLEDGMENTS

We would like to thank the personnel of Stockholm University for the help with the operation of the ECR source. This work was funded by the European network ITS-LEIF, the K&A Wallenberg foundation, and the Swedish Research Council (VR). H.Q.Z. acknowledges the financial support by the National Natural Science Foundation of China (Grant No. 11475075).

[1] N. Stolterfoht, J. H. Bremer, V. Hoffmann, R. Hellhammer, D. Fink, A. Petrov, and B. Sulik, Phys. Rev. Lett. **88**, 133201 (2002).
[2] R. Hellhammer, P. Sobocinski, Z. D. Pešić, D. Fink, J. Bundesmann, B. Sulik, and N. Stolterfoht, Nucl. Instrum. Methods Phys. Res., Sect. B **233**, 213 (2005).
[3] G. Víkor, R. R. Kumar, Z. D. Pešić, N. Stolterfoht, and R. Schuch. Nucl. Instrum. Methods Phys. Res., Sect. B **233**, 218 (2005).
[4] M. B. Sahana, P. Skog, G. Vikor, R. T. Rajendra Kumar, and R. Schuch, Phys. Rev. A **73**, 040901(R) (2006).
[5] S. Mátéfi-Tempfli, M. Mátéfi-Tempfli, L. Piraux, Z. Juhász, S. Biri, É. Fekete, I. Iván, F. Gáll, B. Sulik, G. Víkor, J. Pálinkás, and N. Stolterfoht, Nanotechnology **17**, 3915 (2006).
[6] P. Skog, I. L. Soroka, A. Johansson, and R. Schuch, Nucl. Instrum. Methods Phys. Res., Sect. B **258**, 145 (2007).
[7] Y. Kanai, M. Hoshino, T. Kambara, T. Ikeda, R. Hellhammer, N. Stolterfoht, and Y. Yamazaki, Nucl. Instrum. Methods Phys. Res., Sect. B **258**, 155 (2007).
[8] N. Stolterfoht, R. Hellhammer, Z. Juhász, B. Sulik, V. Bayer, C. Trautmann, E. Bodewits, A. J. de Nijs, H. M. Dang, and R. Hoekstra. Phys. Rev. A **79**, 042902 (2009).
[9] D. Li, Y. Wang, Y. Zhao, G. Xiao, D. Zhao, Z. Xu, and F. Li, Nucl. Instrum. Methods Phys. Res., Sect. B **267**, 469 (2009).
[10] Y.-F. Chen *et al.*, Chin. Phys. B **18**, 2739 (2009).
[11] Z. Juhász, B. Sulik, S. Biri, I. Iván, K. Tőkési, É. Fekete, S. Mátéfi-Tempfli, M. Mátéfi-Tempfli, G. Víkor, E. Takács, and J. Pálinkás, Nucl. Instrum. Methods Phys. Res., Sect. B **267**, 321 (2009).
[12] M. Kreller, G. Zschornak, and U. Kentsch, J. Phys.: Conf. Ser. **163**, 012090 (2009).
[13] N. Stolterfoht, R. Hellhammer, Z. Juhász, B. Sulik, E. Bodewits, H. M. Dang, and R. Hoekstra, Phys. Rev. A **82**, 052902 (2010).
[14] Z. Juhász, B. Sulik, R. Rácz, S. Biri, R. J. Bereczky, K. Tőkési, Á. Kövér, J. Pálinkás, and N. Stolterfoht, Phys. Rev. A **82**, 062903 (2010).

[15] T. Ikeda, Y. Kanai, T. M. Kojima, Y. Iwai, T. Kambara, Y. Yamazaki, M. Hoshino, T. Nebiki, and T. Narusawa, Appl. Phys. Lett. **89**, 163502 (2007).
[16] A. Cassimi, L. Maunoury, T. Muranaka, B. Huber, K. R. Dey, H. Lebius, D. Lelièvre, J. M. Ramillon, T. Been, T. Ikeda, Y. Kanai, and T. M. Kojima, Nucl. Instrum. Methods Phys. Res., Sect. B **267**, 674 (2009).
[17] R. Bereczky, G. Kowarik, F. Aumayr, and K. Tőkési, Nucl. Instrum. Methods Phys. Res., Sect. B **267**, 317 (2009).
[18] G. Kowarik, R. J. Bereczky, F. Aumayr, and K. Tőkési, Nucl. Instrum. Methods Phys. Res., Sect. B **267**, 2277 (2009).
[19] A. R. Milosavljević, G. Víkor, Z. D. Pešić, P. Kolarž, D. Šević, B. P. Marinković, S. Mátéfi-Tempfli, M. Mátéfi-Tempfli, and L. Piraux, Phys. Rev. A **75**, 030901(R) (2007).
[20] S. Das, B. S. Dassanayake, M. Winkworth, J. L. Baran, N. Stolterfoht, and J. A. Tanis, Phys. Rev. A **76**, 042716 (2007).
[21] K. Schiessl, W. Palfinger, K. Tőkési, H. Nowotny, C. Lemell, and J. Burgdörfer, Phys. Rev. A **72**, 062902 (2005).
[22] K. Schiessl, W. Palfinger, K. Tőkési, H. Nowotny, C. Lemell, and J. Burgdörfer, Nucl. Instrum. Methods Phys. Res., Sect. B **258**, 150 (2007).
[23] K. Schiessl, C. Lemell, K. Tőkési, and J. Burgdörfer, J. Phys.: Conf. Ser. **163**, 012081 (2009).
[24] K. Schiessl, K. Tőkési, B. Solleder, C. Lemell, and J. Burgdörfer, Phys. Rev. Lett. **102**, 163201 (2009).
[25] P. Skog, H. Q. Zhang, and R. Schuch, Phys. Rev. Lett. **101**, 223202 (2008).
[26] Y. Kanai, M. Hoshino, T. Kambara, T. Ikeda, R. Hellhammer, N. Stolterfoht, and Y. Yamazaki, Phys. Rev. A **79**, 012711 (2009).
[27] N. Stolterfoht, R. Hellhammer, D. Fink, B. Sulik, Z. Juhász, E. Bodewits, H. M. Dang, and R. Hoekstra, Phys. Rev. A **79**, 022901 (2009).
[28] H. Q. Zhang, P. Skog, and R. Schuch, Phys. Rev. A **82**, 052901 (2010).
[29] H. Q. Zhang, N. Akram, P. Skog, I. L. Soroka, C. Trautmann, and R. Schuch, Phys. Rev. Lett. **108**, 193202 (2012).
[30] H. Q. Zhang, N. Akram, I. L. Soroka, C. Trautmann, and R. Schuch, Phys. Rev. A **86**, 022901 (2012).
[31] H. Q. Zhang, N. Akram, I. L. Soroka, C. Trautmann, and R. Schuch, J. Phys.: Conf. Ser. **488**, 012035 (2014).
[32] S. Winecki, C. L. Cocke, D. Fry, and M. P. Stöckli, Phys. Rev. A **53**, 4228 (1996).
[33] O. B. Firsov, Sov. Phys.-Dokl. **11**, 732 (1967).
[34] A. Arnau, F. Aumayr, P. M. Echenique, M. Grether, W. Heiland, J. Limburg, R. Morgenstern, P. Roncin, S. Shippers, R. Schuch, N. Stolterfoht, P. Varga, T. J. M. Zouros, and H. P. Winter, Surf. Sci. Rep. **27**, 113 (1997).
[35] M. J. Simon, C. L. Zhou, M. Döbeli, A. Cassimi, I. Monnet, A. Méry, C. Grygiel, S. Guillous, T. Madi, A. Benyagoub, H. Lebius, A. M. Müller, H. Shiromaru, and H.-A. Synal, Nucl. Instrum. Methods Phys. Res., Sect. B **330**, 11 (2014)